
THERMODYNAMIC & PATTERN-MATCHING EFFICIENCY IN HETEROGENEOUS NETWORKS

A PREPRINT

Daive Cipollini^{*,1,2}, Lambert Schomaker^{1,2}

¹ Bernoulli Institute for Mathematics, Computer Science and Artificial Intelligence,
University of Groningen, Nijenborgh 9, 9747 AG Groningen, The Netherlands

² Cognigron - Groningen Cognitive Systems and Materials Center,
Nijenborgh 9, 9747 AG Groningen, The Netherlands

Email: d.cipollini@rug.nl and l.r.b.schomaker@rug.nl

ABSTRACT

Why complex structures emerge in a real world environment is a fascinating question which has not found any fully satisfactory answer at the point of today. At the border between statistical physics, machine learning and network theory, we provide some computational empirical evidence indicating that the emergence of complex structures in the outer world is the macroscopic thermodynamic result of the optimal trade-off between the ability to encode information about the environment in the very features of the network and the ability to transmit information across it. While the former is quantified by the von Neumann network entropy and the latter by the Helmholtz free energy, the two are combined into a single quantity tantamount to the thermodynamic efficiency. We take as a case study an algorithm originally proposed for creating and searching trees of patterns under the assumption that, akin to living system, the algorithm seeks the best internal representation of the outer world, namely a real world dataset of patterns. Remarkably, the optimal thermodynamic efficiency overlaps with the optimal pattern-matching efficiency, defined in terms of accuracy and computational cost, whether the former is measured at the resolution scale where the network transits from exhibiting a specific heat with a single peak to a scale-invariant region. Moreover the critical hypothesis is investigated and empirical evidence suggests that the system benefits from the vicinity to the critical point whether it is faced with higher-complexity environments, while it does not when the environment is simpler.

Keywords von Neumann entropy · Specific heat · Thermodynamics · Statistical physics · Machine Learning

1 Introduction

Why complex structures emerge in a real world environment is a fascinating question which has not found any fully satisfactory answer at the point of today. We aim at some computational empirical evidence suggesting that the emergence of complex structures is the macroscopic thermodynamic result of the optimal ability to store the information about the environment in an accessible manner with the ability to transmit information across the structure [1, 2]. The latter is defined in terms of microscopic quantities thanks to the fairly newly developments in statistical physics of fields in network theory [2, 3, 4, 5]. In living systems, natural selection is the way the information about the environment flows into the system's genome which will then encode such information in the structural traits of the organisms which in turn reflect the functional capability of the system. Thus the structural traits of a system could themselves enclose the complexity of the environmental conditions the system needs to adapt to, or in other words, to represent into its very own structure [6]. How these traits are optimized to maximize the fitness to the environment is an open question. The hypothesis of optimal functioning at the border of order and disorder suggests the critical point as the potential candidate to obtain functional advantages [7, 8, 9, 10, 11] and maximize the fitness to the outer world, or to obtain

a better performance in a statistical generalization problem in the context of learning machines. Here we challenge this hypothesis. In our work a system seeks the best-fitness configuration given some external constraints r and a high-dimensional vector collection, the dataset \mathcal{D} .

We take as case study the algorithm introduced by Portegys [12] for accelerating nearest-neighbour (1-NN) pattern recognition tasks and subsequently extended to k-NN [13]. The algorithm employs a tree formation protocol where raw data are reorganized into tree structures using a recursive tree-formation method in which samples are randomly selected and inserted into the growing tree structure. At each step the new pattern is linked to either the currently parent pattern or to one of the k-NN children of the parent pattern. The choice is based on the relative distance between the parent and the new pattern and the one evaluated between the child pattern and the new pattern. The parameter r modulates the relative importance of these two distances creating a larger or smaller region of influence of the parent in the sample space. Figure 1 shows the three structure prototypes produced depending on the value of the control parameter r . For $r \sim 0$, every node is linked to the root node (see the central node, which is the first node selected in the process) and a star graph turns out. For some intermediate value of r a ragged tree structure is produced, while for $r \rightarrow 2$ a 1d-lattice is created. Remarkably, the algorithm produces exclusively trees, i.e. number of spanning trees is always 1, which are sparse $|E| = N - 1$ where $|E|$ and N are the number of links and nodes respectively. Using the metaphor introduced by Jacob for natural selection¹ [14], the algorithm does act as a *tinkerer* that creates a structure using what is available at the time, collocating one node after the other across the tree formation process according to a distance based rule.

Depending on the structural traits of the networks, an optimal trade-off between fast search of the best-matching pattern and accuracy in terms of node-class labels can be defined.

The Portegys algorithm has the desirable properties of being simple, explainable and subject to a single control parameter r . Thanks to these features, we can work on the bridge between three disciplines: statistical physics, machine learning and network science, and we can show that information-theoretical tools such as the von Neumann entropy and its derivative reflect the functional capabilities of the network. Most notably thermodynamic efficiency and pattern-matching efficiency demonstrate noticeable overlap.

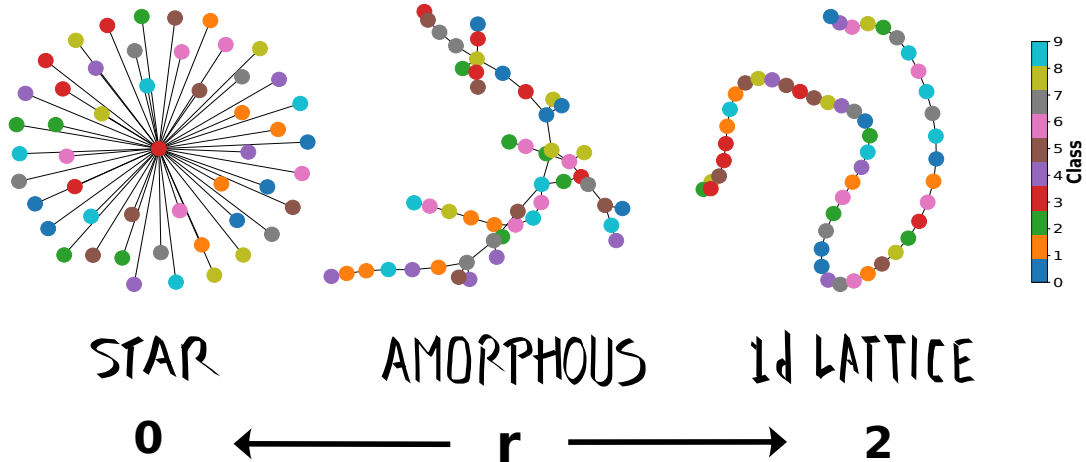


Figure 1: **The three prototypical structures generated by the Portegys algorithm.** The algorithm creates star-like networks up to 1d lattice when $r \rightarrow 2$. For intermediate values of r , networks resembling an arborescent tree are produced. The process is reminiscent of the transition *vapor/liquid* \rightarrow *amorphous solid* \rightarrow *1d lattice*. Depicted networks are generated from a subset of 50 samples randomly extracted from the MNIST dataset with $r = 0.05, 0.95, 1.50$ respectively. Classes are indicated by the 10 different colors in the color-bar.

¹

"Natural selection does not work as an engineer works. It works like a tinkerer - who does not know exactly what he is going to produce but uses whatever he finds around him whether it be pieces of string, fragments of wood, or old cardboard; in short works like a tinkerer who uses everything at his disposal to produce some kind of workable object."

2 Theoretical framework

2.1 Statistical physics of networks

Information spreading over networked structures is governed by the Laplacian matrix [15] and its spectrum of eigenvalues encodes many relevant topological properties of the graph [16, 17]. Let us consider an undirected and unweighted network $G(V, E)$ of order $|V| = N$ with number of links equal to $|E| = m$. The network Laplacian is defined as $\hat{L} = \hat{D} - \hat{A}$, where \hat{D} and \hat{A} are the diagonal matrix of the node degrees and the adjacency matrix respectively. The Laplacian operator can be used to define a density operator [5], where the Laplacian takes the role of the Hamiltonian of statistical physics [18] as in Equation (1).

Given an initial state of the network encoding the concentration of quantity, e.g. information, in one or more nodes, $\underline{s}(0)$, the state at time τ is given by $\underline{s}(\tau) = e^{-\tau\hat{L}}\underline{s}(0)$. Where $\hat{K} = e^{-\tau\hat{L}}$ is the network propagator and is the discrete counterpart of the path integral formulation for general diffusion processes [19, 20].

As \hat{K} is a positive semidefinite Hermitian matrix admits the spectral decomposition in terms of the sum of projectors $\hat{K} = \sum_i^N e^{-\tau\lambda_i} |k_i\rangle\langle k_i|$. Thus, for any state at τ it holds $|\phi(\tau)\rangle = \sum_i^N e^{-\tau\lambda_i} |k_i\rangle\langle k_i| |\phi(0)\rangle$. This relation remarks that the eigenvectors of the Laplacian are akin to the wave-vectors in the Fourier space defined by the spectrum of the continuum-Laplacian, while τ can be interpreted as the "wave length" $l \sim \tau$ of the diffusion modes, thus it defines an operational resolution scale for observations [3]. Moreover, the ensemble of accessible diffusion modes at time τ can be constructed defining a probability measure over the accessible modes decomposed by the spectral theorem. Such canonical ensemble [5, 4, 21] is encoded into the density matrix:

$$\hat{\rho}_\tau = \frac{e^{-\tau\hat{L}}}{Z} \quad (1)$$

The elements ρ_{ij} represent the normalized amount of information transferred in a diffusion process between nodes i and j at time τ . Remarkably ρ_{ij} takes into account all possible topological pathways between the two nodes and assigns smaller weights to longer ones tantamount to path-integrals [19, 21]. The partition function $Z = \text{Tr}[\hat{K}] = \sum_{i=1}^N e^{-\tau\lambda_i(\hat{L})}$ is a function of the eigenvalues, λ_i , of the Laplacian and is proportional to the average return probability of a continuous time edge-centric random walker to be back in its initial location at time τ [4]. Note that the object $\hat{\rho}$ is a positive semi-definite and Hermitian matrix whose trace sums to unity which has allowed its eigenvalues to be interpreted as probabilities.

Finally, the network von Neumann entropy can be introduced [5] as a multi-scale descriptor of the network structure:

$$S(\hat{\rho}(\tau)) = - \sum_{i=1}^N \mu_i(\tau) \log \mu_i(\tau) \quad (2)$$

where $\{\mu_i(\tau)\}_{i=1}^N$ is the set of $\hat{\rho}(\tau)$ eigenvalues that are related to the set of Laplacian eigenvalues through $\mu_i(\tau) = e^{-\tau\lambda_i}/Z$. The entropy $S(\hat{\rho}(\tau))$ is a function of the normalized time τ and is bounded between $[\log C_{conn}, \log N]$ where C_{conn} is the number of connected components and N is the number of nodes. Thus the von Neumann entropy S as a function of τ reflects the *entropic phase transition* of information propagation (or loss) over the network [21] as illustrated in Figure 2. Specifically for a connected network, at $\tau \rightarrow 0$, $S(\tau) = \log N$ reflects the segregated heterogeneous phase where information diffuses from the single nodes to the very local neighborhood; at $\tau \rightarrow \infty$, $S(\tau) = 0$ the diffusion is governed by the smallest non-zero eigenvalue of the Laplacian, associated with the so-called Fiedler eigenvector, reflecting the homogeneous phase where the information has propagated all over the network.

The network entropy thus counts the (logarithmic) number of informationally connected components on the heterogeneous network and by the inspection of the entropy S and its generalized susceptibility (or specific heat) $C = -dS/\log \tau$ it is possible to identify the characteristic resolution scales of the network [21, 3]. For instance, a constant specific heat reflects the scale-invariance of the network where information is lost at a constant rate. Such a situation is typical of d-dimensional lattices and scale invariant networks with power law distributed spectrum. On the contrary, a single large peak of the specific heat C identifies a single scale where there is a fast and unique information diffusion (or information lost) across the network. The latter is the typical situation of a star graph, depicted in Figure 1, or an Erdős-Rényi network, see purple curve in Figure 1. Before the peak the informationally connected components are the single nodes and after the peak the informationally connected components are the full-network revealing a single trivial-scale.

From this considerations, a Laplacian-Renormalization group theory has been recently developed allowing for a coarse-graining of the network structures into super-nodes unraveling the mesoscale structures [3, 21]. In this context,

the peaks of the specific heat, C , or a marked change in its slope, identify the most convenient resolution scales where to perform the coarse-graining over the *informationally connected* nodes, as it allows the iteration of the procedure without an excessive network reduction.

To conclude, we can intuitively use the diffusion parameter τ to resolve the network topological structures at different resolution scales. Thus, the necessity of analyzing complex networked systems at all levels is solved by resorting to the conjugate Fourier space, the k -space, defined by the Laplacian spectrum and the "wavelengths" of its modes.

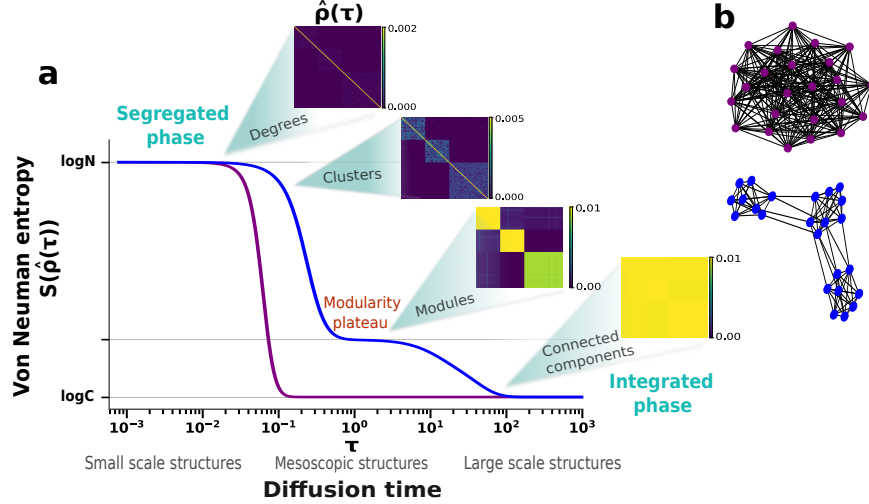


Figure 2: **Von Neumann entropy as a function of the diffusion time.** Panel (a) depicts diffusion over two exemplary networks with analogous topological features to those depicted in panel (b): in blue a stochastic block model network exhibiting tripartite modular structure, and in purple a Erdős-Rényi random network with the same number of nodes of the blue one. For small $\tau \sim 0$, both networks exhibit the maximum spectral entropy value $\log N$, where N is the number of nodes, reflecting the segregated phase. For $\tau \rightarrow \infty$, the spectral entropy converges to $\log C$, where C is the number of connected components, thus reflecting the integrated phase. For intermediate values of τ , the Erdős-Rényi network shows a single critical scale at which the network transitions from the segregated to the integrated phase. The position on the horizontal axis of the critical scale is related to the edge density of the network as well as the heterogeneity in the degree distribution. On the contrary, the blue network exhibits two critical resolution scales in the entropic transition. At smaller τ , information initially diffuses within the modules ending into a plateau. A later slower diffusion process between the three modules completes the transition to the integrated phase. The insets show the density matrix $\hat{\rho}_\tau$ across the entropic transition on the blue curve. The tripartite modular structure of the network is shown by the emergence of the three blocks in the density matrix. Graphs depicted in (b) have only illustration purpose. Illustration from [22, 21, 23].

2.2 Thermodynamics of networks

The statistical physics theory for networks introduced above naturally allows to view network phenomena from a new perspective and to bridge the gap to network macroscopic observables. To this regard network thermodynamic quantities as work, W , and heat, Q , can be defined in (at least mathematical) analogy to their thermodynamic counterparts [2]. Since a network of isolated nodes is the only network with maximum entropy $S_{iso} = \log N$ for $\tau > 0$, progressively adding edges results in diminishing the entropy of the network. In turns, lower entropy reflects the diminished ability of the network to express diversity to a stochastic perturbation, or in other terms, the loss in the internal representation capabilities encoded in the network topological traits. The entropic cost is given by:

$$Q = -\frac{dS}{\tau} = -\frac{\log N - S}{\tau} \leq 0 \quad (3)$$

which resembles the heat dissipation in a thermodynamic process.

On the other hand, it is obvious that adding edges increases the information flow quantified by the (Helmholtz) free energy $F = -\log Z/\tau$ [2, 4]. Less obvious is how, for a fixed number of edges, the degree distribution influences the flow of information. As the Laplacian governs the continuous-time *edge-centric* random walk, the presence of

large hubs implies an enhancement of the process with faster propagation of the diffusing quantity [15, 24]. As the free energy is inversely related to the partition function, $Z = \sum_{i=1}^N e^{-\tau\lambda_i}$, the bounds of the former are given by the bounds of the latter. From $1 \leq Z \leq N$, where the lower bound is given for the connected network at large $\tau \gg 1$, while the upper bound is given by a network of isolated nodes $\forall\tau$, or for a connected one at small scales $\tau = 0$. Thus, the $-\log N/\tau \leq F \leq 0$ and the gain in information flow is reflected by the variation of the free energy from the case of isolated nodes:

$$W = dF = F - F_{iso} = F + \frac{\log N}{\tau} \geq 0 \quad (4)$$

which is tantamount to the work in the canonical ensemble. Moreover, $U = W + Q \geq 0$ which implies $W \geq |Q|$. A formation process can be depicted as the trade-off between these two necessities of the networked complex system: the need to maximize the information flow, while at the same time retaining an amount of structural entropy such that the network can encode and express sufficient diversity through its traits.

Thus, to complete the analogy to thermodynamics, the trade-off between diversity of information and information flow is captured by the efficiency [2]:

$$\eta = \frac{W + Q}{W} = 1 - \frac{|Q|}{W} = \frac{U}{W} \quad (5)$$

where $0 \leq \eta \leq 1$ and $U \equiv -\partial_\tau \log Z \equiv \text{Tr}[\hat{L}\hat{\rho}]$. The variational principle here exposed has been devised to macroscopically explain the sparsity and its empirical scaling law, as well as the emergence of topological features such as modularity, small-worldness and heterogeneity [2]. In our work we make use of this variational principle to explain the structural properties of a network that is required to encode the diversity expressed in the environment, where the environment is defined by a real-world dataset of patterns. We also make use of the specific heat to identify which is the resolution scale at which such variational principle is effective for heterogeneous networks constrained to a sparsity regime.

3 Methods

Our results are evaluated over subsets of three different datasets: the NIST [25], the MNIST [26] and the FashionMNIST [27] datasets. These datasets contain randomly collected instances of image samples out of 10 classes. It should be noted that in this type of data, a pattern class can generally not be represented by a single centroid vector, but will contain multiple densities ('sub-style patterns') such that the sample point cloud can be ordered naturally in a network structure. The MNIST database contains 24×24 grey-scale images of handwritten digits [0-9] commonly used to benchmark machine- and deep- learning algorithms. The NIST dataset is the ancestor of the MNIST, it contains 16×16 black-and white images of the handwritten digits [0-9]. The FashionMNIST is a large dataset of 28×28 gray-scale images of fashion products from 10 categories. In all our experiments a subset of 2000 samples is extracted from the train-set and the test-set independently. In the Supplementary we show also the same results for larger networks generated from 4000 samples from the MNIST and FashionMNIST. The 10 classes are equally represented both in the test and in training set. We limit to $r \leq 0.85$ as the accuracy, and hence the pattern-matching efficiency quickly drops for larger r , moreover the algorithm shows instability as it doesn't necessarily converge for $r \geq 0.9$. The Portegys algorithm we use is the extended version with $k = 5$ introduced in [13] and where distance between patterns is the Euclidean distance.

3.1 Pattern-matching efficiency

After the tree formation described in Section 1, the Portegys algorithm enters the search phase, where the best match to a test pattern is given using a first-best approach. The original goal of this algorithm was to restructure a list of examples in a tree-based way, such that the matching accuracy would not be much worse than nearest-neighbor matching on a full list, while providing a considerable speed up due to the tree-based structure. The search process is an iterative process which begins with the computation of the distance between the test pattern and the root-node pattern scaled by r . The distance is then compared to the distance between the test pattern and all of the root node's children. The first node with a pattern that has a smaller distance is than selected as the new root node, and the process starts over with the newly selected node as root. The search phase terminates when no node whose pattern has smaller distance to the test pattern than the current one can be found.

It is natural to define an pattern-matching efficiency, θ , in terms of class match accuracy, A , and the number of distances computed, N_{dist} :

$$\theta = \frac{A}{\log N_{dist}} \quad (6)$$

the logarithm is taken since the range of N_{dist} can virtually span the interval $N_{dist} \in (0, N]$ where N is the number of nodes. For the case of a star graph, $r \rightarrow 0$, the number of computed distances is maximum $N_{dist} = N$, for lower values of r the number of computed distances decreases as does the accuracy but at a different pace, thus, it is possible to identify an optimal trade-off between the gain in computational burden and the loss in performance, as depicted in panel (c) of Figure 3.

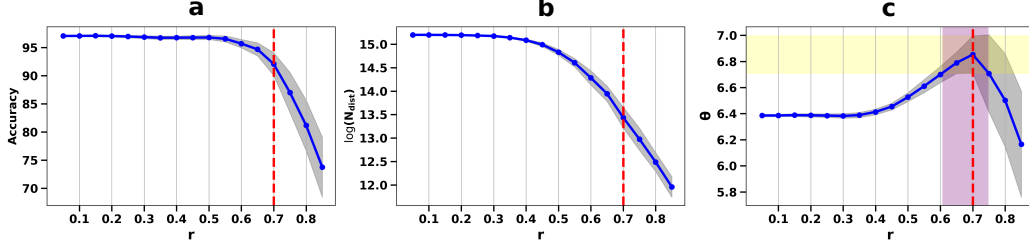


Figure 3: **Pattern-matching efficiency**, (c), is defined as the trade-off between the classification accuracy, (a), and the logarithm of the number of distances computed to find the best match, (b). The dashed-red vertical line indicates the optimal r value in terms of efficiency. The shaded grey area designates the standard deviation. The purple shaded area in panel (c) indicates a tolerance r -domain of optimal efficiency. The tolerance domain is defined as the r -values such that the corresponding θ -values are included in one standard deviation computed at the maximum θ , whose y-axis projection is indicated by yellow shaded area. Curves are computed over 50 independent simulations with a subset of 2000 samples extracted from the NIST dataset. The 10 digit-classes are equally represented both in the train- and test-set.

4 Results

4.1 Thermodynamic and pattern-matching efficiency at the emergence of new C-peaks

Figure 4 shows the coherence between algorithmic defined in Section 3 and thermodynamic efficiency in Equation (5) for the three investigated datasets. In panels (a)-(c) the pattern-matching efficiency, θ , is depicted. The vertical red-dashed line indicates the r value for the optimal algorithmic trade-off, while the shaded purple region indicates a r -domain tolerance of the optimal pattern-matching efficiency. The tolerance domain is defined as the r -values such that the corresponding θ -values are included in one standard deviation computed at the best trade-off. In panels (d)-(f) the thermodynamic efficiency, η , shows remarkable overlap with the pattern-matching efficiency θ in terms of optimal r . See the r -range spanned by the purple-shaded areas in panels (a)-(c) and the vertical dashed lines in panels (d)-(f). The overlap between the two efficiencies suggests that, whether thermodynamic or algorithmic, the two objects are the same thing just viewed from different angles. See the next Section for the discussion on the double peak of the η curves for the MNIST.

Similar to what would be the transition from vapor/liquid to an amorphous solid, at a critical value of r topological complexity increases from the trivial traits of a star graph. Thus, the emergence of structure is reflected by the arise of a second peak in C together with a roughly $C = c_0 > 0$ plateau in between the first and the last peak as is illustrated in panels (e)-(i). Such transition is also depicted in Figure 5 by the bifurcation of the blue and green curves for $\tau_{peak}^{(1)}$ and for $\tau_{peak}^{(2)}$ indicating the lower and upper branches in panels (g)-(i) of Figure 4.

Before the bifurcation the two curves overlap and the single peak in the specific heat identifies a single trivial resolution scale below which the informationally connected components are the single nodes, and after which the informationally connected component is the full graph. The emergence of a plateau $C = c_0 > 0$ for $r \rightarrow 2$ reflects the emergence of a progressively larger scale invariant structure. For $r \rightarrow 2$ we expect the plateau height to converge to the theoretical value $C \rightarrow c_0 = 1/2$ of the 1d-lattice passing by $c_0 = 4/6$ for random trees notoriously related to the spectral dimension $d = 2c_0$ [3]. See also Section S4 illustrating the spectral entropy and specific heat curves for the three datasets independently depicted for each r -value.

Remarkably, the thermodynamic efficiency is computed at the specific resolution scale $\tau \sim 10$ involved in the structural transition. Such critical resolution scale is identified by the bifurcation of the specific heat peaks depicted in panels (e)-(i) of Figure 4 and in panels (a)-(c) of Figure 5. In the seminal work [2], it is indicated to compute the thermodynamics efficiency, η , using as a reference the τ -scale equal to the inverse of the Fiedler eigenvalue, i.e. the smallest non-zero Laplacian eigenvalue $\lambda_2 = 1/\tau_{diff}$, as this provides the time-scale where the diffusion process has reached equilibrium

according to the authors, and then logarithmically divide τ_{diff} to progressively define the large propagation scales, the middle scales and the small scales.

Nevertheless, τ_{diff} only approximates the end of the diffusion process which is better reflected by $\tau_{peak}^{(2)}$. Panels (a)-(c) of Figure 5 show the τ_{diff} in red next to the $\tau_{peaks}^{(1,2)}$ curves discussed above. The key difference is in the use of the ensemble average which employs all the eigenvalues to compute the specific heat. Thus, it is crucial to identify which is the τ -scale which resolves the phase transition from the single trivial scale of the star graph to more complex topological traits of the amorphous network depicted in Figure 1. Such resolution scale is the relevant scale for the computation of the efficiency η and defines an "ultra-violet" cut-off in the characteristic frequency of the network across the transformation, similarly to what was discussed in the context of the Laplacian-Renormalization group [3]. In Section S3 the efficiency, η , is computed in the range interval indicated by the diffusion time as defined in [2] $\tau_{diff} = 1/\lambda_2$, i.e. the red curves depicted in panels (a). Whether computed at those scales, η shows a change in concavity and no consistent relation with the algorithmic accuracy.

Moreover note in Figure 5 the slow down of diffusion indicated by the $\tau_{peak}^{(2)}$ curve as a function of r , we remark that $\tau_{peak}^{(2)}$ is a function of the parameter r only which shapes the degree distribution as the number of nodes and edges is fixed across the transition. We remind that the Portegy's algorithm allows us to stay in the regime of sparsity, symbolically $\delta(\frac{N-1}{|E|} - 1)$.

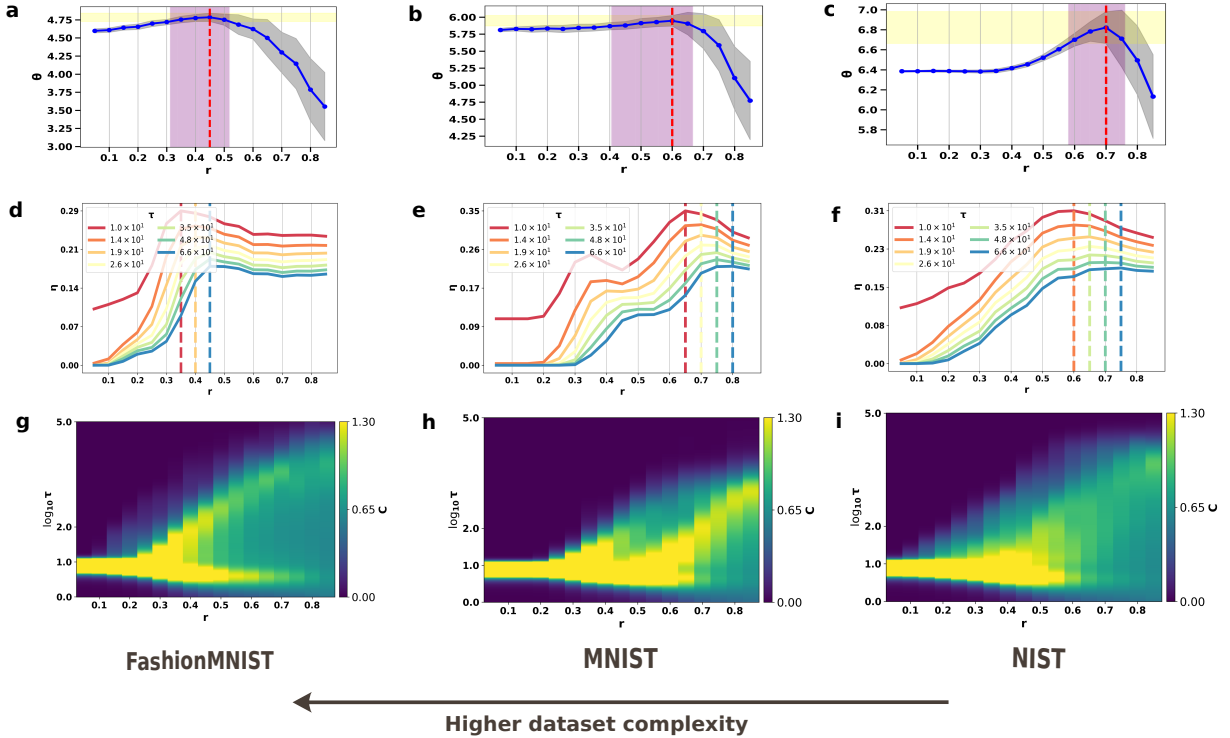


Figure 4: **Thermodynamic & pattern-matching efficiency.** In (a)-(c) the pattern-matching efficiency, θ , is plotted as a function of r for the three investigated datasets of increasing complexity (see arrow at the bottom of the figure). The shaded purple area indicates the tolerance r -range for the optimal pattern-matching efficiency, which includes points in one standard deviation from the global maximum indicated by the vertical red-dashed line. In (d)-(f) the optimal thermodynamic efficiency, η , as a function of r overlaps with the pattern-matching efficiency. Vertical dashed-lines indicate the global maxima of the efficiencies. Remarkably, the thermodynamic efficiency is measured in the τ -range of one order of magnitude from the bifurcation of the specific heat, C , depicted in panels (g)-(i). The τ -resolution scale $\tau \sim 10$ identifies the relevant length scale resolving the transition from the single-peak to the emergence of a roughly plateau region, $C = c_0 > 0$, reflecting a roughly scale-invariant structure. Note that for datasets of higher complexity the highest efficiency, both thermodynamic and algorithmic, are posited at the critical value of the structural phase transition illustrated by the specific heat in panels (g)-(i). This is in line with the argument that states that a fairly simple dataset does not benefit from the critical point. Quantities are averaged over 50 independent simulations.

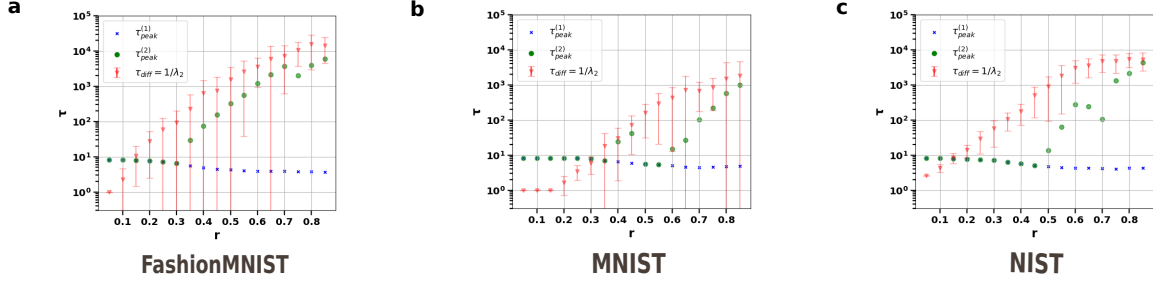


Figure 5: **Role of the ensemble average on the estimation of the τ -scale.** Panels (a)-(c) depict the $\tau_{peak}^{(1,2)}$ and τ_{diff} as a function of r . $\tau_{peak}^{(1,2)}$ are the τ -location of the first and last peak of the specific heat in Figure 4. τ_{diff} is the Fiedler eigenvalue which provides a good estimation of the end of the diffusion process only for sufficiently large r . Note that the red curves retrace the profile of the upper branch of the specific heat for $\tau \gtrsim 10$ in panels (g)-(i) of Figure 4. At smaller r values the equilibrium time is better reflected by $\tau_{peak}^{(2)}$. The equilibrium of the diffusion process is an increasing function of r . τ_{diff} curves are averaged over 50 independent simulations. The $\tau_{peak}^{(1,2)}$ curves are computed from the specific heat curves which are averaged over 50 independent simulations.

4.2 Performance at criticality

As previously discussed, the τ -scale where the bifurcation in panels (e)-(i) of Figure 4 and in panels (a)-(c) of Figure 5 shows up indicates the scale involved in the structural transition and it is the resolution scale where the thermodynamic efficiency overlaps with the pattern-matching efficiency as a function of r . Nevertheless, the critical value of r where such structural transition appears is not necessarily the value where the efficiencies have the global maximum.

To discuss this empirical result we turn our attention to the panels (a)-(c) in Figure 4 and panels (a)-(c) in Figure 5. While for the FashionMNIST dataset there is a rough correspondence between the $r \sim 0.30$ where the structural transition emerges and the r -range $r \in (0.30, 0.50)$ where the global maximum of the efficiencies is observed, for the MNIST and NIST datasets the thermodynamic and algorithmic efficiencies show a maximum in ranges of r which are farther away from the respective bifurcation points $r \sim 0.35$ and $r \sim 0.45$. The term "far away" is quantified by the purple-shaded areas Figure 4. We rather observe in panels (b), (c), (e) and (f) of Figure 4 that the maximum efficiencies are posited where the $\tau_{peak}^{(2)}$ have a discontinuous jump in panels (b), (c) of Figure 5 at $r \sim 0.60$ for the MNIST and at $r \sim 0.70$ for the NIST. The argument holds also for the MNIST if we include θ points in the one standard deviation illustrated by the shaded-purple area. The jump for the MNIST curve in Figure 5 is such that the two $\tau_{peak}^{(1,2)}$ curves overlap. We mention that this effect is mitigated for larger datasets, i.e. larger networks, as we show in Section S2 of the Supplementary. The jump is caused by the presence of a third large peak in between $\tau^{(1)}$ and $\tau^{(2)}$ (see Figure 4 and the entropy curves depicted in Figure S6). Moreover, for the MNIST case, the jump is sufficiently strong to be reflected on a local maximum in the efficiency, η . Even though this local maximum in η is not registered by the averaged pattern-matching efficiency θ in Figure 4(b), it is reflected in its standard deviation which allows us to include the r -range indicated by the shaded purple area, which corresponds to the η -peak-to-peak r -range in Figure 4(e).

Nevertheless, we stress once again that we did not compute the thermodynamic efficiency at the corresponding τ scale where discontinuity of the $\tau_{peak}^{(2)}$ curve appears, but we rather measured η at the τ scale indicated by the bifurcation.

To explain the diversity in the positioning of the maximum of the efficiencies, either in the vicinity of the transition point or farther away, we turn to the argument, already present in the literature [28, 10, 29], that indicates the necessity of tuning a system, or of a system to self-tune, at the border of a phase transition only when the task requires a high level of complexity. While for the FashionMNIST, a notoriously more complex dataset when compared to both the MNIST and NIST, the optimal value for the efficiency is posited in the proximity of the critical value of $r \sim 0.30$, the optimal values of r for the NIST and MNIST datasets are evidently far away from their respective transition values. The MNIST, which is the intermediate dataset in terms of complexity, is an interesting case as it shows two maxima for the thermodynamic efficiency η . While the global maximum in Figure 4(e) is far away from the critical value of r illustrated by the bifurcation in panel (b) of Figure 5, the local maxima is at $r \sim 0.35 - 0.40$ which corresponds to the critical value of r indicated by the bifurcation. This observation is in line with the hypothesis that the system

takes advantage from the critical behaviour only when a fairly complex task is presented to it and in line with other observations discussed in the literature [28, 10]. Thus, it stresses the importance of dataset under analyses.

Moreover, while the value of r where a structural transition appears is dependent on the dataset, i.e. $r = .45$ for the NIST, $r = .35$ for the MNIST and $r = .30$ for the FashionMNIST, the $\tau \sim 10^1$ scale identified is the same for all the three datasets. Interestingly, the τ -scale is also unaffected by the number of nodes in the network (see Supplementary Section S2). We speculate about the possibility that this is due to the constraint on sparsity as it is an invariant feature over the cases investigated in this manuscript.

5 Discussion

The ability of a system to survive is the capability of concentrating a flow of order from the environment - “drinking order from the environment” [30]. In other words, systems, whether living systems or machine(-learning) systems, need to learn an efficient internal representation of the complex world - or the dataset- they are posed in contact with. Such internal representation can be encoded in terms of abstract probability distributions [9, 10] or in the very network-features of the system, as it happens in genetic regulatory networks playing a central role in morphogenesis [31], or in a mixed-way as in artificial neural networks where the engineer designs a complicated distribution through the definition of an architecture and the training phase fills in the parameters in order to obtain the desired function-approximation machine to achieve statistical generalization [32].

When confronted to real world environment, in order to survive, living systems not only need the capability of interpreting the environment, but they also need the capability to quickly react with a coherent response to stimuli possibly drawn from the same distribution they adapted to [33]. Moreover the same system needs to cope with cost of sending information across its structure which can cause an enhanced exploitation of resources. In the context of machine-learning, cost can be quantified by the number of computations to be done before the satisfying answer to the task can be reported, e.g. class-matching. By using the recently developed theoretical tools of statistical physics of fields for networks [5, 4, 34, 21, 3, 2], we have quantified the diversity in the traits of the network with the von Neumann entropy and the transmission flow of information with the Helmholtz free energy. As fastness of information flow and sufficiently rich representation of the outer world are two competing capabilities, the formation process of a complex networked structure is interpreted as the macroscopic thermodynamic outcome of the delicate balance between the two, and a variational principle in terms of thermodynamic efficiency can be devised to explain why a certain structure emerge in place of an other [2]. We have shown that such a thermodynamic efficiency strikingly overlaps with the pattern-matching efficiency defined in terms of accuracy and computational costs, suggesting that the two can be regarded as the same thing but viewed from different angles.

Notably, we have shown that the thermodynamic efficiency needs to be computed at a specific resolution scale τ . We have used the specific heat $C = -dS/d \log \tau$ to identify the τ -resolution which resolves the transition from the trivial-structure, that is a single specific heat peak, to emergence of more complex structures, where the specific heat shows some plateau reflecting the growth of a scale-invariant region where information is integrated at a constant rate. Such τ -resolution scale is akin to an “ultra-violet” cut-off delimiting the frequency of the network structure across the heterogeneity-transition from star graph to 1d-lattice trough amorphous. While the transition point reflects the network resolution scale where the thermodynamic efficiency needs to be measured, the corresponding transition value of the control parameter r does not coincide with the global maximum in efficiency. We explain this with the statement that a system benefits from the critical point only when it confronts with environments of higher complexity, while it does not benefit from it when the environmental complexity is lower. This is elucidated by the use of three different datasets of increasing complexity and supported by other works in the literature [28, 10, 29].

Conflict of Interest Statement

The authors declare that the research was conducted in the absence of any commercial or financial relationships that could be construed as a potential conflict of interest.

Author Contributions

DC: Theoretical framework, Conceptualization, Methodology, Simulations, Data curation, Software, Writing – original draft, Writing – review & editing. LS: Writing – review & editing, Conceptualization, Supervision, Funding acquisition.

Funding

This work was funded by EUs Horizon 2020, from the MSCA-ITN-2019 Innovative Training Networks program "Materials for Neuromorphic Circuits" (MANIC) under the grant agreement No. 861153, as well as by the financial support of the CogniGron research center and the Ubbo Emmius Funds (Univ. of Groningen).

Acknowledgments

We are thankful to Jos van Goor for providing some of the scripts that enabled efficient grid-search across parameters and to Federico Balducci for the useful discussions.

Supplemental Data

Supplementary Material include figures that are mentioned in the main text but are omitted from it to the purpose of clarity.

Data Availability Statement

The original contributions presented in the study are included in the article/supplementary material, further inquiries can be directed to the corresponding author/s. Datasets and scripts can be found at https://github.com/CipolliniDavide/Laplacian_Trees.

References

- [1] Eörs Szathmáry and John Maynard Smith. The major evolutionary transitions. *Nature*, 374(6519):227–232, March 1995.
- [2] Arsham Ghavasieh and Manlio De Domenico. Diversity of information pathways drives sparsity in real-world networks. *Nature Physics*, 20(3):512–519, January 2024.
- [3] Pablo Villegas, Tommaso Gili, Guido Caldarelli, and Andrea Gabrielli. Laplacian renormalization group for heterogeneous networks. *Nature Physics*, 2023.
- [4] Arsham Ghavasieh, Carlo Nicolini, and Manlio De Domenico. Statistical physics of complex information dynamics. *Phys. Rev. E*, 102:052304, 2020.
- [5] Manlio De Domenico and Jacob Biamonte. Spectral entropies as information-theoretic tools for complex network comparison. *Physical Review X*, 6(4), 2016.
- [6] Manlio De Domenico. Exploring evolution (in life) through information. <https://substack.com/home/post/p-143130785?source=queue>, April 2024. Accessed: 2024-04-16.
- [7] Chris G. Langton. Computation at the edge of chaos: Phase transitions and emergent computation. *Physica D: Nonlinear Phenomena*, 42(1–3):12–37, June 1990.
- [8] Nils Bertschinger and Thomas Natschläger. Real-time computation at the edge of chaos in recurrent neural networks. *Neural Computation*, 16(7):1413–1436, July 2004.
- [9] Iacopo Mastromatteo and Matteo Marsili. On the criticality of inferred models. *Journal of Statistical Mechanics: Theory and Experiment*, 2011(10):P10012, October 2011.
- [10] Jorge Hidalgo, Jacopo Grilli, Samir Suweis, Miguel A. Muñoz, Jayanth R. Banavar, and Amos Maritan. Information-based fitness and the emergence of criticality in living systems. *Proceedings of the National Academy of Sciences*, 111(28):10095–10100, June 2014.
- [11] Bryan C. Daniels, Hyunju Kim, Douglas Moore, Siyu Zhou, Harrison B. Smith, Bradley Karas, Stuart A. Kauffman, and Sara I. Walker. Criticality distinguishes the ensemble of biological regulatory networks. *Physical Review Letters*, 121(13), September 2018.
- [12] T.E. Portegys. A search technique for pattern recognition using relative distances. *IEEE Transactions on Pattern Analysis and Machine Intelligence*, 17(9):910–914, 1995.
- [13] Mangalagiu D. *Accélération de l’algorithme des k plus proches voisins par réorganisation arborescente de la base de données*. PhD thesis, Ecole Polytechnique, Paris, 1999.

- [14] François Jacob. Evolution and tinkering. *Science*, 196(4295):1161–1166, June 1977.
- [15] Naoki Masuda, Mason A. Porter, and Renaud Lambiotte. Random walks and diffusion on networks. *Physics Reports*, 716-717:1–58, 2017.
- [16] William N. Anderson and Thomas D. Morley. Eigenvalues of the laplacian of a graph. *Linear and Multilinear Algebra*, 18(2):141–145, 1985.
- [17] Ernesto Estrada. *The Structure of Complex Networks: Theory and Applications*. Oxford University Press, Inc., USA, 2011.
- [18] Mehran Kardar. *Statistical Physics of Fields*. Cambridge University Press, June 2007.
- [19] Richard P. Feynman. *Statistical Mechanics: A Set Of Lectures*. CRC Press, 1998.
- [20] Paolo Moretti and Michael Zaiser. Network analysis predicts failure of materials and structures. *Proceedings of the National Academy of Sciences*, 116(34):16666–16668, August 2019.
- [21] Pablo Villegas, Andrea Gabrielli, Francesca Santucci, Guido Caldarelli, and Tommaso Gili. Laplacian paths in complex networks: Information core emerges from entropic transitions. *Physical Review Research*, 4(3), 2022.
- [22] Carlo Nicolini, Giulia Forcellini, Ludovico Minati, and Angelo Bifone. Scale-resolved analysis of brain functional connectivity networks with spectral entropy. *Neuroimage*, 211(116603):116603, 2020.
- [23] Davide Cipollini, Anede Swierstra, and Lambert Schomaker. Modeling a domain wall network in bifeo3 with stochastic geometry and entropy-based similarity measure. *Frontiers in Materials*, 11, January 2024.
- [24] Chittaranjan Hens, Uzi Harush, Simi Haber, Reuven Cohen, and Baruch Barzel. Spatiotemporal signal propagation in complex networks. *Nature Physics*, 15(4):403–412, January 2019.
- [25] Patrick Grother. Nist special database 19 handprinted forms and characters database. 1995.
- [26] Li Deng. The mnist database of handwritten digit images for machine learning research. *IEEE Signal Processing Magazine*, 29(6):141–142, 2012.
- [27] Han Xiao, Kashif Rasul, and Roland Vollgraf. Fashion-mnist: a novel image dataset for benchmarking machine learning algorithms, 2017.
- [28] Benjamin Cramer, David Stöckel, Markus Kreft, Michael Wibral, Johannes Schemmel, Karlheinz Meier, and Viola Priesemann. Control of criticality and computation in spiking neuromorphic networks with plasticity. *Nature Communications*, 11(1), June 2020.
- [29] Alireza Goudarzi, Christof Teuscher, Natali Gulbahce, and Thimo Rohlf. Emergent criticality through adaptive information processing in boolean networks. *Physical Review Letters*, 108(12), March 2012.
- [30] Erwin Schrodinger and Roger Penrose. *What is Life?: With Mind and Matter and Autobiographical Sketches*. Cambridge University Press, March 2012.
- [31] Dmitry Krotov, Julien O. Dubuis, Thomas Gregor, and William Bialek. Morphogenesis at criticality. *Proceedings of the National Academy of Sciences*, 111(10):3683–3688, February 2014.
- [32] Yoshua Bengio. *Deep Learning*. Adaptive Computation and Machine Learning series. MIT Press, London, England, November 2016.
- [33] Raviv Pryluk, Yoav Kfir, Hagar Gelbard-Sagiv, Itzhak Fried, and Rony Paz. A tradeoff in the neural code across regions and species. *Cell*, 176(3):597–609, 2019.
- [34] Arsham Ghavasieh and Manlio De Domenico. Generalized network density matrices for analysis of multiscale functional diversity. *Phys. Rev. E*, 107:044304, 2023.

SUPPLEMENTARY INFORMATION: THERMODYNAMIC & PATTERN-MATCHING EFFICIENCY IN HETEROGENEOUS NETWORKS

A PREPRINT

Daive Cipollini^{*,1,2}, Lambert Schomaker^{1,2}

¹ Bernoulli Institute for Mathematics, Computer Science and Artificial Intelligence,
University of Groningen, Nijenborgh 9, 9747 AG Groningen, The Netherlands

² Cognigron - Groningen Cognitive Systems and Materials Center,
Nijenborgh 9, 9747 AG Groningen, The Netherlands

Email: d.cipollini@rug.nl and l.r.b.schomaker@rug.nl

Keywords von Neumann entropy · Specific heat · Thermodynamics · Statistical physics · Machine Learning

S1 Laplacian spectrum

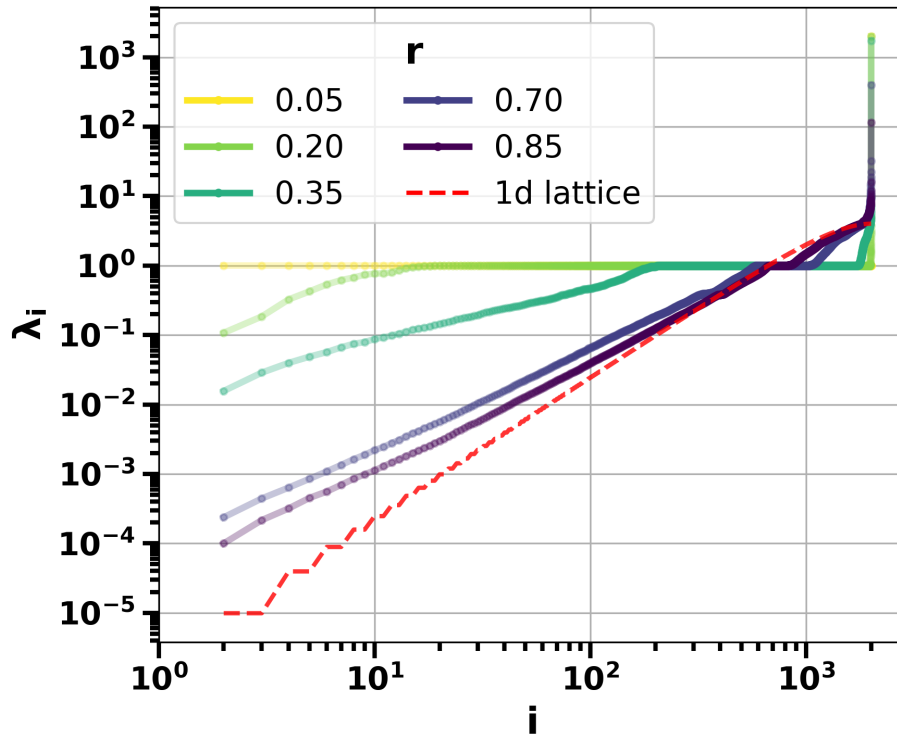


Figure S1: **Laplacian spectrum** for multiple values of r . The red-dashed line indicates the limit of 1-d dimensional lattice converging towards a power law with exponent $\gamma = 2$, corresponding to the plateau height of the specific heat $c_0 = 1/\gamma$ in the limit of continuous spectrum. The greater is the degeneracy in the eigenvalue spectrum larger is the peak in the specific heat (see Figure S6). For the case of the star graph $r = 0.05$ the maximum eigenvalue is equal to the maximum number of nodes $\lambda_{max} = 2000$. Points are averaged over 50 independent network generations from the subset of 2000 FashionMNIST samples.

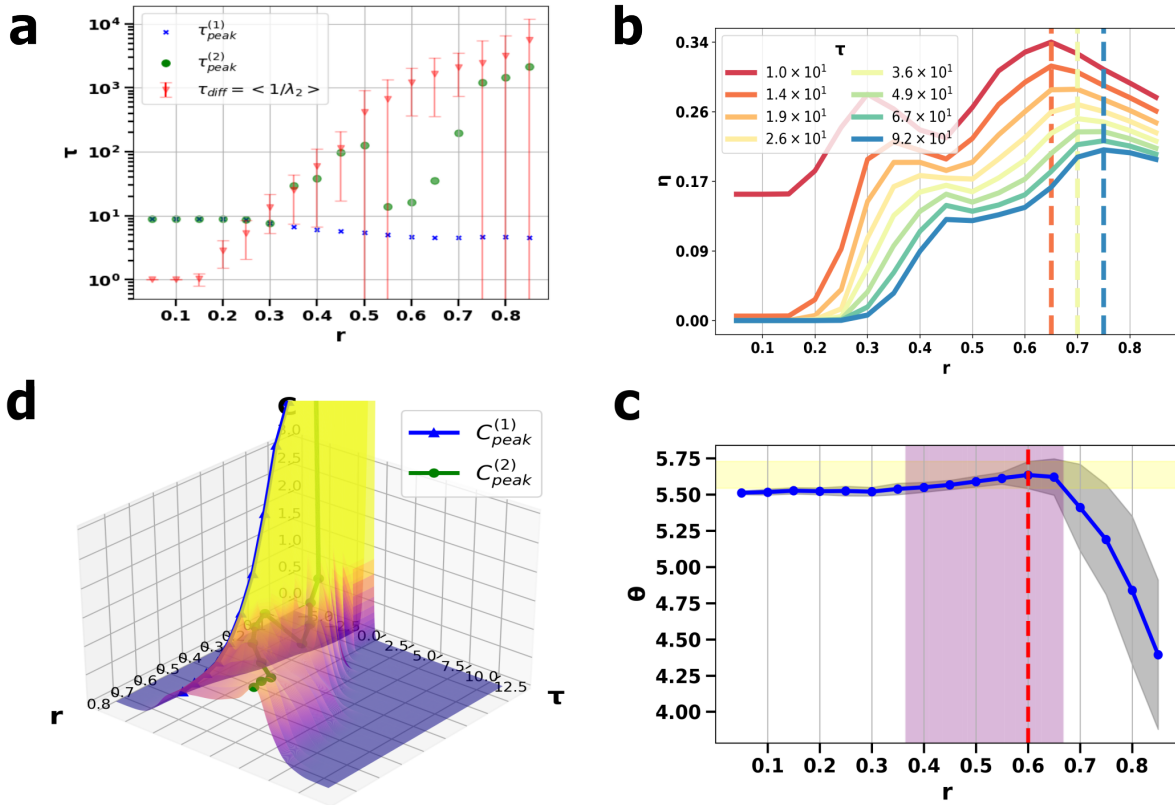
S2 Larger networks: N=4000


Figure S2: **MNIST - N=4000**. In (a) the bifurcation of $\tau_{peak}^{(1)}$ and $\tau_{peak}^{(2)}$ curves identify the τ -scale relevant for the topological transition. The jump of $\tau_{peak}^{(2)}$ towards $\tau_{peak}^{(1)}$ is less pronounced compared to networks of 2000 nodes. In red the numerical average of the diffusion time $1/\tau_{diff} = \lambda_2$ is plotted for reference, see the main text for discussion. In (d) the specific heat, C , surface is illustrated. The $C_{peak}^{(1,2)}$ curves correspond to the specific heat values evaluated along the curves $\tau_{peak}^{(1,2)}$ in (a). In (b)-(c) the efficiencies η and θ are plotted as a function of r with the dashed-lines indicating the global maxima. The η is computed in the τ -range of one order of magnitude from the τ -scale indicated by the bifurcation of $\tau_{peak}^{(1,2)}$ in (a). For larger networks N=4000 optimal r remains unchanged as it is a property mostly dependent on the dataset complexity. Shaded area in (c) spans over the two local maxima in panel (b) (see main text for discussion). Quantities are averaged over 50 independent simulations.

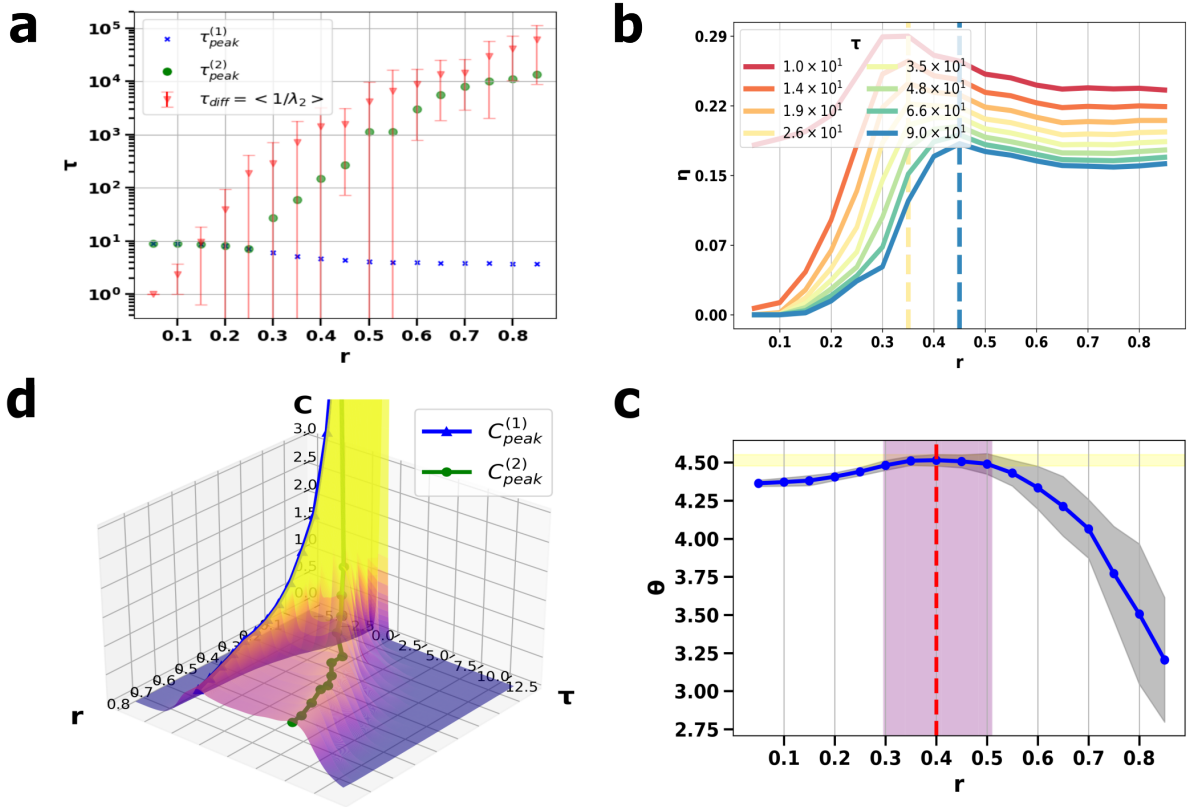


Figure S3: **FashionMNIST - N=4000**. In (a) the bifurcation of $\tau_{peak}^{(1)}$ and $\tau_{peak}^{(2)}$ curves identify the τ -scale relevant for the topological transition. The red curve depicts the numerical average of the diffusion time $1/\tau_{diff} = \lambda_2$, see the main text for discussion. In (d) the specific heat, C , surface is illustrated. The $C_{peak}^{(1,2)}$ curves correspond to the specific heat values evaluated at $\tau_{peak}^{(1,2)}$ in (a). In (b)-(c) the efficiencies η and θ are plotted as a function of r with the dashed-lines indicating the global maxima. The η is computed in the τ -range of one order of magnitude from the τ -scale indicated by the bifurcation of $\tau_{peak}^{(1,2)}$ in (a). Note that the maxima of the efficiencies is posited at the edge of the critical value of $r \sim 0.35$ indicating the FashionMNIST as a dataset more complex than the other two investigated, that does benefit from the critical region. Quantities are averaged over 50 independent simulations.

S3 Thermodynamic efficiency change in concavity

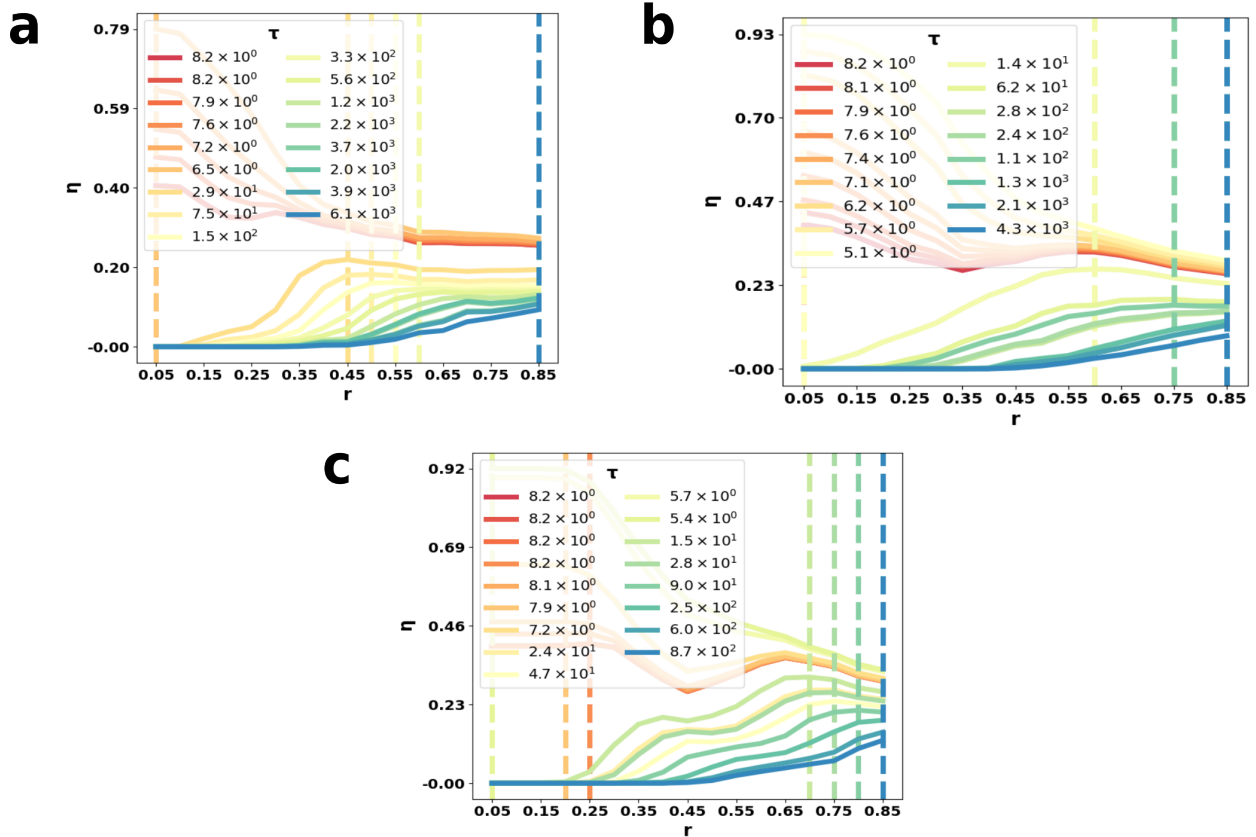


Figure S4: **Thermodynamic efficiency changes concavity for τ smaller than the transition resolution scale.** Remarkably, the coherence between thermodynamic and algorithmic efficiency is lost for resolution τ -scales above and below the order of magnitude where the transition appears, i.e. $\tau \sim 10$. Panels (a)-(c) show the transition for trees of order $N = 2000$, hence 2000 samples from the datasets NIST, FashionMNIST and MNIST. Curves are averaged over 50 independent iterations.

S4 Von Neumann entropy and specific heat

Figures S5-S9 depict the spectral entropy, S in blue, and the specific heat, C in red, for multiple values of the control parameter r . Y-ticks on the right axis correspond to the theoretical specific heat plateau values for an infinite 2d-lattice, tree and 1-d lattice respectively in descending order.

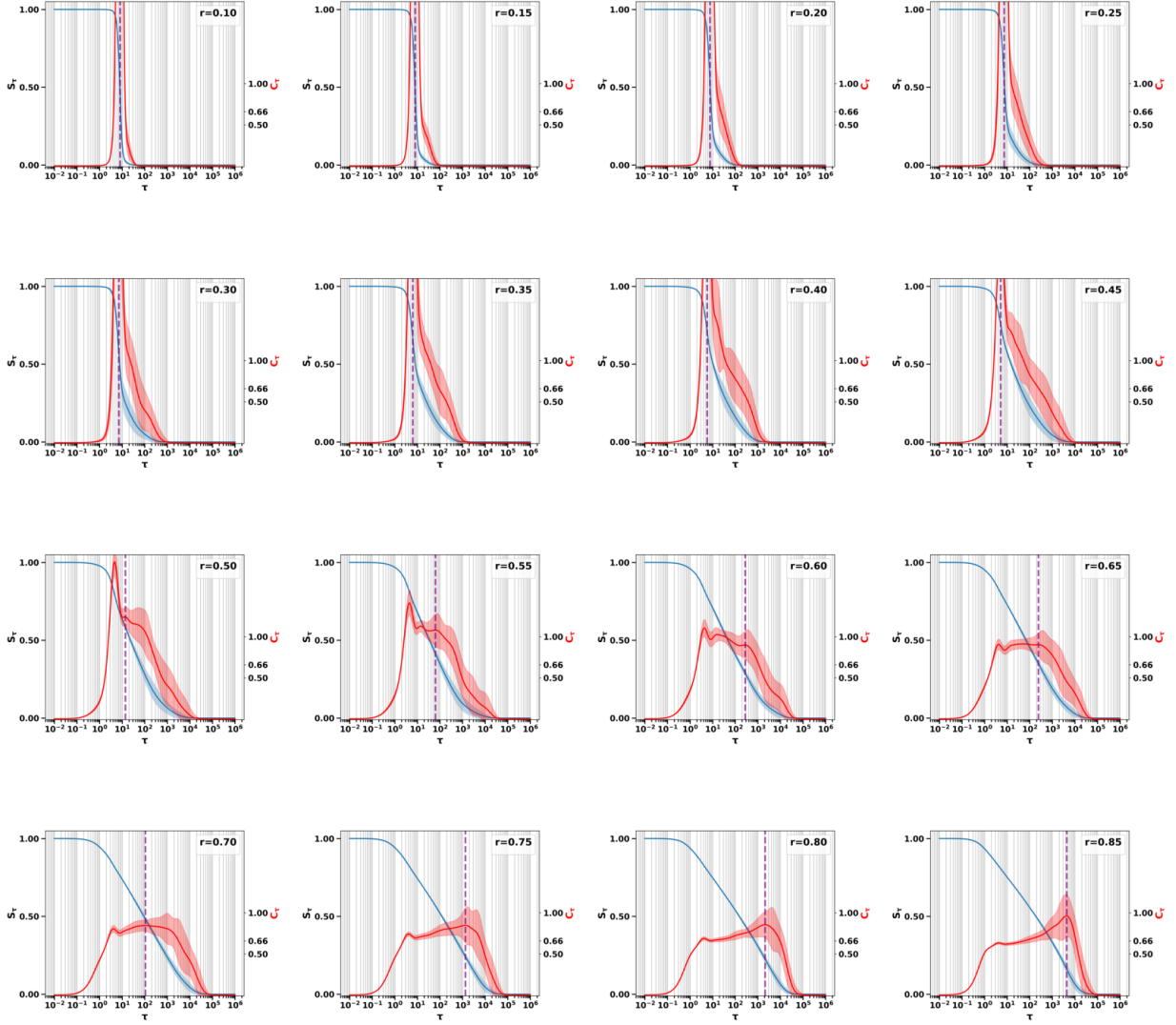


Figure S5: **Von Neumann and specific heat - NIST: 2000 samples.** The table shows the von Neumann entropy (blue) and the specific heat (red) for $r = \{0.10, \dots, 0.85\}$. Vertical dashed lines indicate the peaks corresponding to $\tau_{peak}^{(2)}$ in the main text. Shaded areas represent the standard deviation. Curves are averaged over 50 simulations.

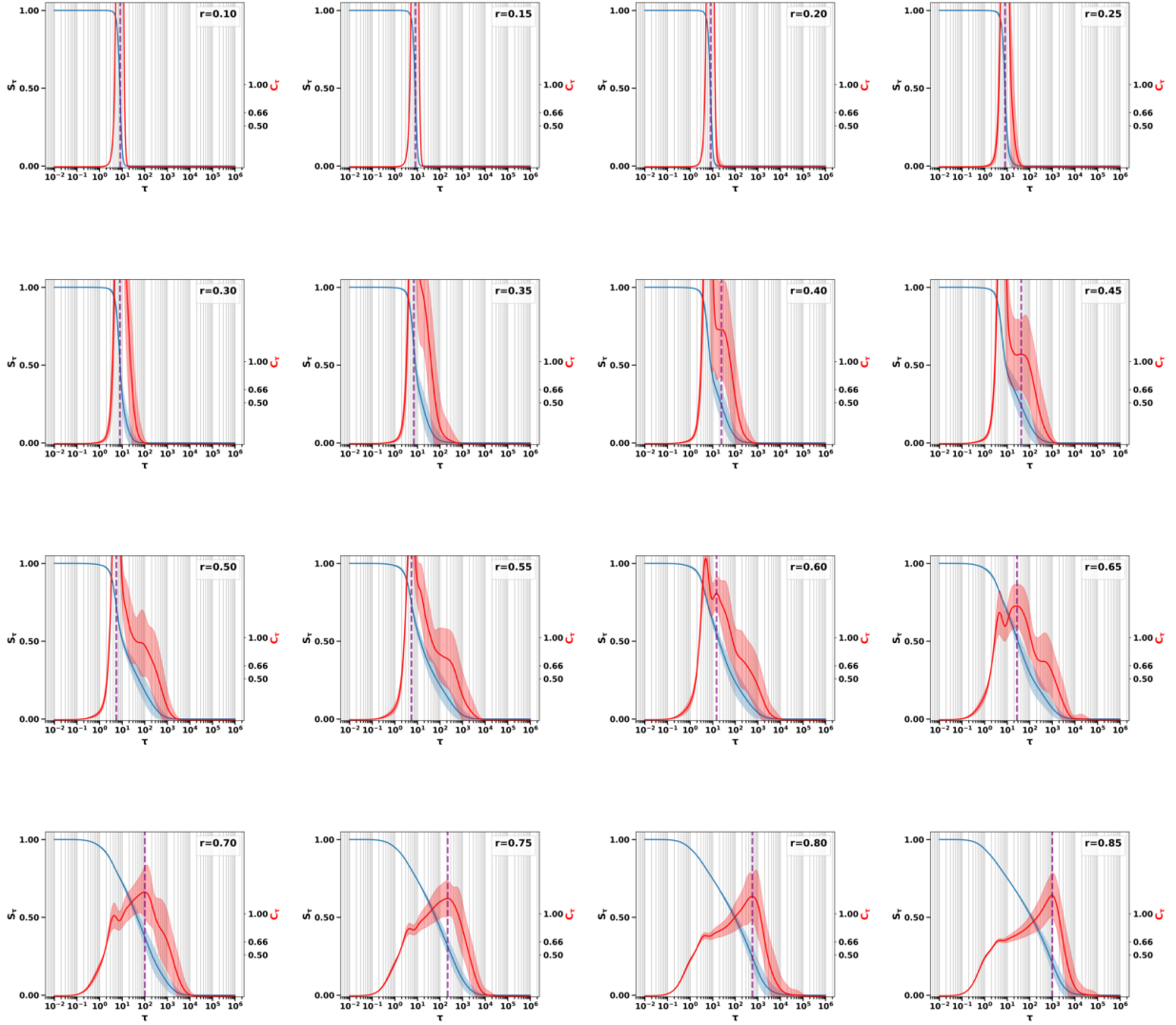


Figure S6: **Von Neumann and specific heat - MNIST: 2000 samples.** The table shows the von Neumann entropy (blue) and the specific heat (red) for $r = \{0.10, \dots, 0.85\}$. Vertical dashed lines indicate the peaks corresponding to $\tau_{peak}^{(2)}$ in the main text. Shaded areas represent the standard deviation. Curves are averaged over 50 simulations.

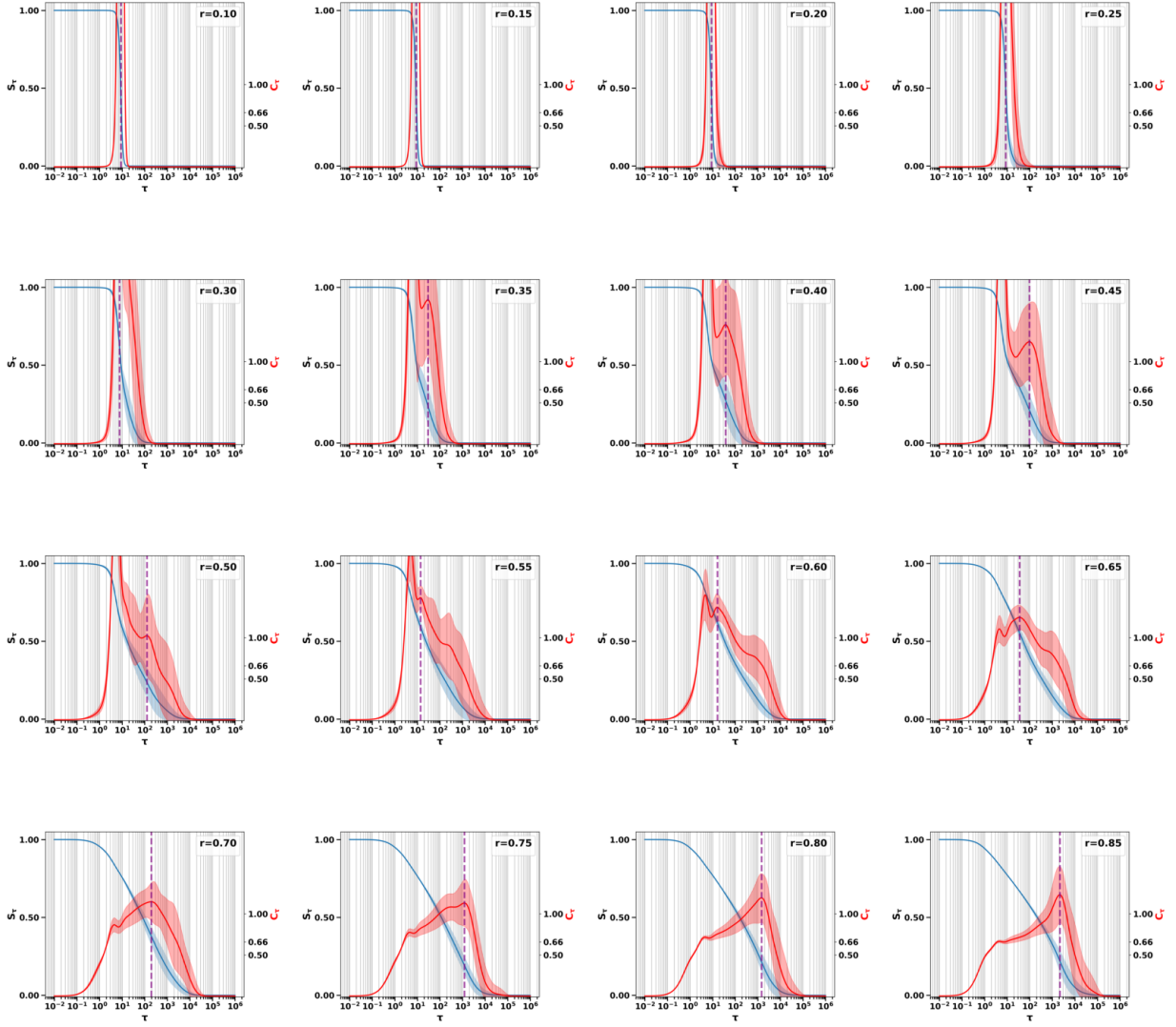


Figure S7: **Von Neumann and specific heat - MNIST: 4000 samples.** The table shows the von Neumann entropy (blue) and the specific heat (red) for $r = \{0.10, \dots, 0.85\}$. Vertical dashed lines indicate the peaks corresponding to $\tau_{peak}^{(2)}$ in the main text. Shaded areas represent the standard deviation. Curves are averaged over 50 simulations.

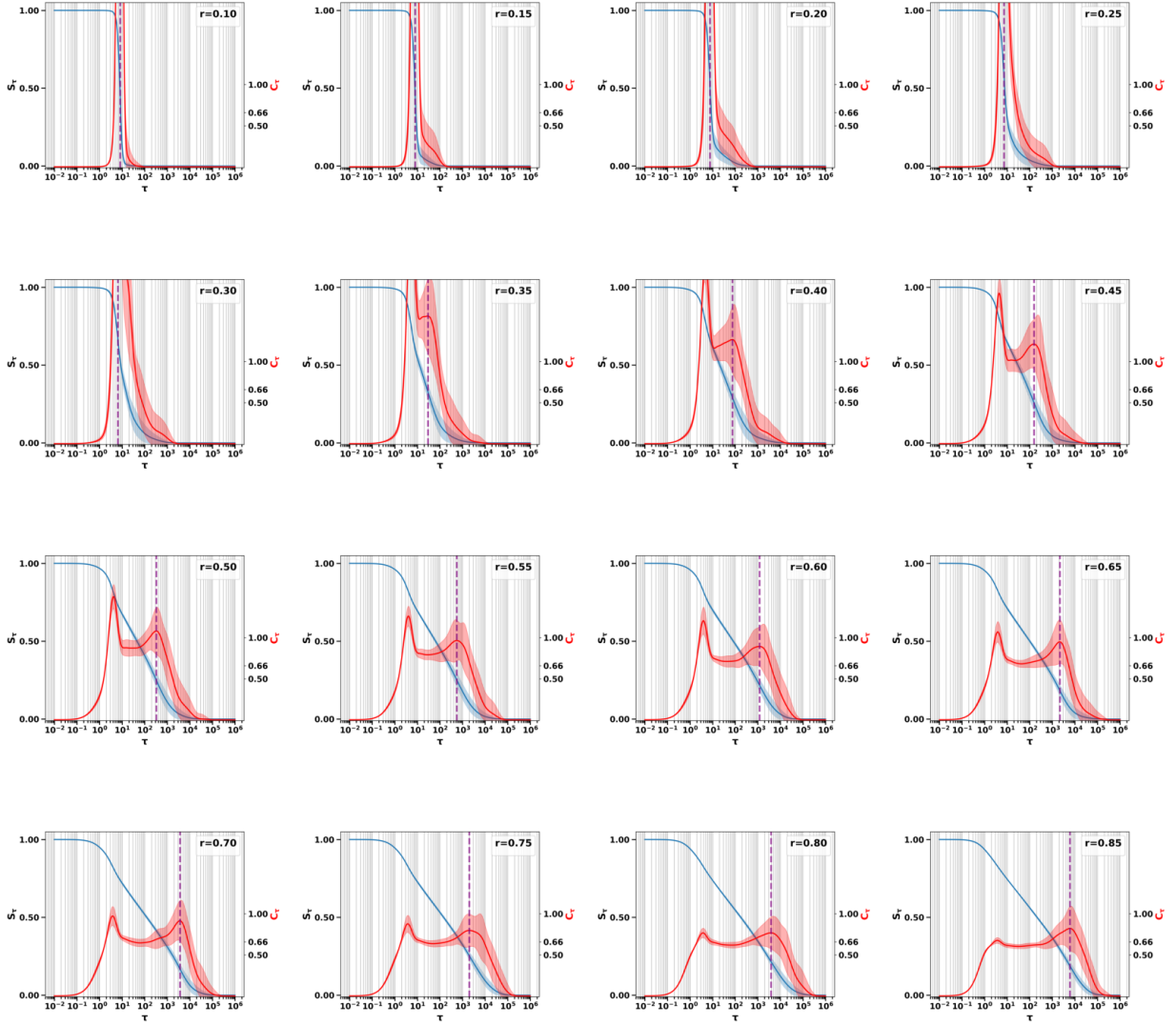


Figure S8: **Von Neumann and specific heat - FashionMNIST: 2000 samples.** The table shows the von Neumann entropy (blue) and the specific heat (red) for $r = \{0.10, \dots, 0.85\}$. Vertical dashed lines indicate the peaks corresponding to $\tau_{peak}^{(2)}$ in the main text. Shaded areas represent the standard deviation. Curves are averaged over 50 simulations.

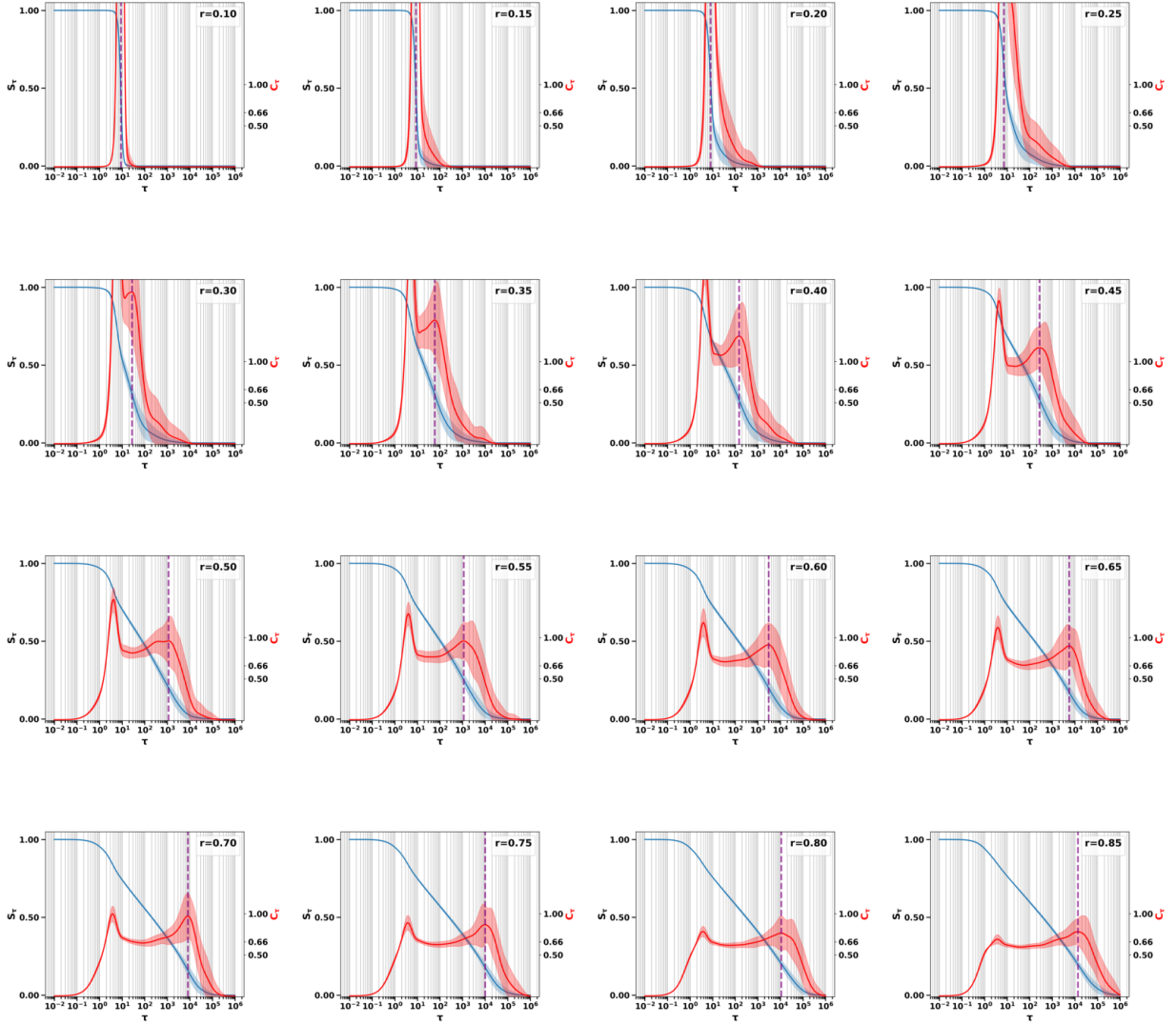


Figure S9: **Von Neumann and specific heat - FashionMNIST: 4000 samples.** The table shows the von Neumann entropy (blue) and the specific heat (red) for $r = \{0.10, \dots, 0.85\}$. Vertical dashed lines indicate the peaks corresponding to $\tau_{peak}^{(2)}$ in the main text. Shaded areas represent the standard deviation. Curves are averaged over 50 simulations.

S5 Variance of F , dF , dS , η

Figure S10 shows the variance of the quantities F , dF , dS , η for the three datasets. The peak of the variance indicates the location of the structural phase transition.

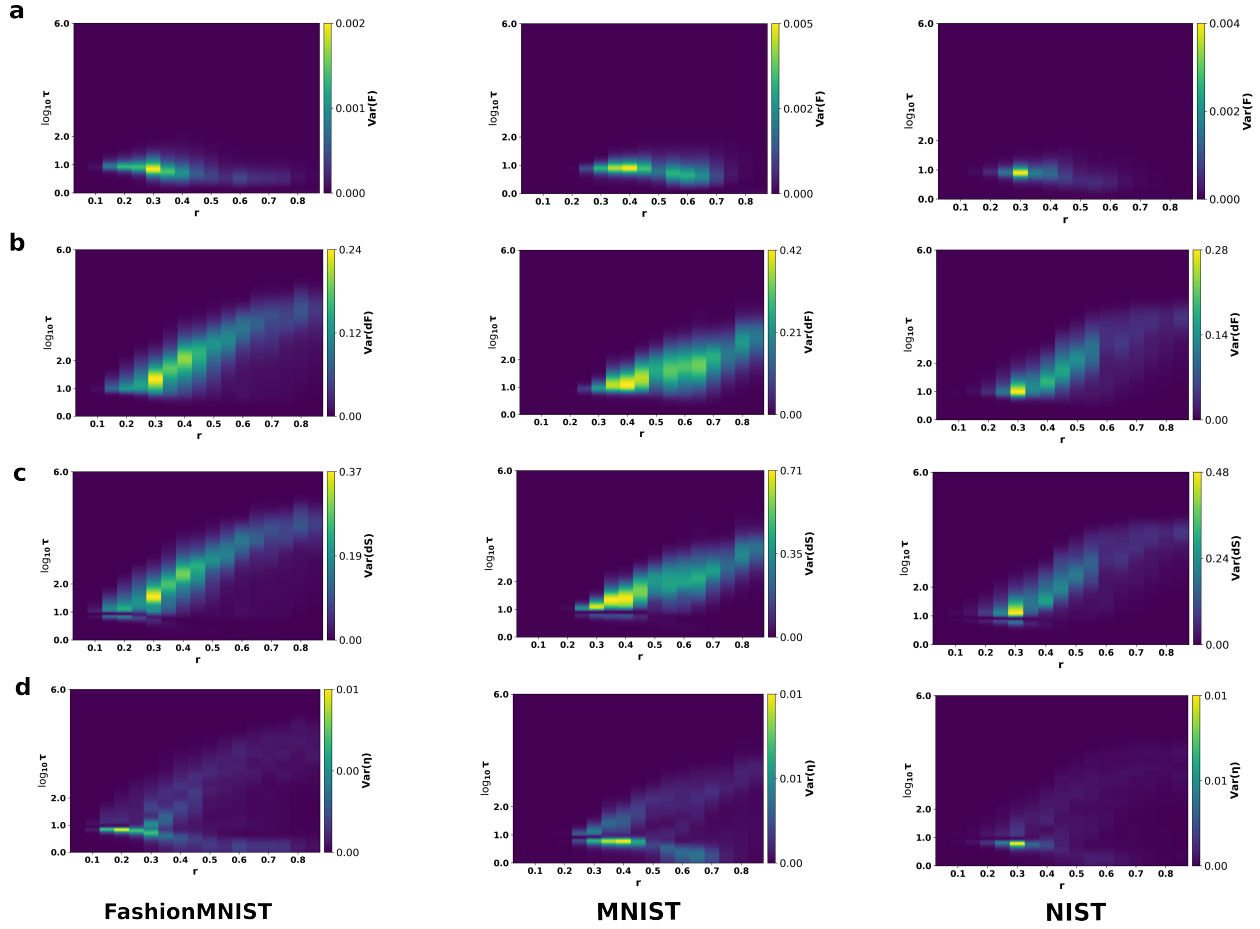


Figure S10: **Variance of F , dF , dS , η - 2000 samples** in panels (a) through (d) for the three datasets (columns). The peaks of the variance indicate the loci of the structural phase transition. Variance computed over 50 independent simulations.

Author Contributions

DC: Theoretical framework, Conceptualization, Methodology, Simulations, Data curation, Software, Writing – original draft, Writing – review & editing. LS: Writing – review & editing, Conceptualization, Supervision, Funding acquisition.

Funding

This work was funded by EUs Horizon 2020, from the MSCA-ITN-2019 Innovative Training Networks program "Materials for Neuromorphic Circuits" (MANIC) under the grant agreement No. 861153, as well as by the financial support of the CogniGron research center and the Ubbo Emmius Funds (Univ. of Groningen).

Acknowledgments

We are thankful to Jos van Goor for providing some of the scripts that enabled efficient grid-search across parameters and to Federico Balducci for the useful discussions.

Data Availability Statement

The original contributions presented in the study are included in the article/supplementary material, further inquiries can be directed to the corresponding author/s. Datasets and scripts can be found at https://github.com/CipolliniDavide/Laplacian_Trees.